



HAL
open science

Electrotrophy as potential primary metabolism for colonization of conductive surfaces in deep-sea hydrothermal chimneys

Guillaume Pillot, Sylvain Davidson, Laetitia Shintu, Oulfat Amin, Anne Godfroy, Yannick Combet-Blanc, Patricia Bonin, Pierre-Pol Liebgott

► **To cite this version:**

Guillaume Pillot, Sylvain Davidson, Laetitia Shintu, Oulfat Amin, Anne Godfroy, et al.. Electrotrophy as potential primary metabolism for colonization of conductive surfaces in deep-sea hydrothermal chimneys. 2020. hal-03022667

HAL Id: hal-03022667

<https://amu.hal.science/hal-03022667>

Preprint submitted on 24 Nov 2020

HAL is a multi-disciplinary open access archive for the deposit and dissemination of scientific research documents, whether they are published or not. The documents may come from teaching and research institutions in France or abroad, or from public or private research centers.

L'archive ouverte pluridisciplinaire **HAL**, est destinée au dépôt et à la diffusion de documents scientifiques de niveau recherche, publiés ou non, émanant des établissements d'enseignement et de recherche français ou étrangers, des laboratoires publics ou privés.

1 **Electrotrophy as potential primary metabolism for colonization of** 2 **conductive surfaces in deep-sea hydrothermal chimneys.**

3 Guillaume Pillot¹, Sylvain Davidson¹, Laetitia Shintu³, Oulfat Amin Ali^x, Anne Godfroy², Yannick Combet-Blanc¹, Patricia
4 Bonin¹, Pierre-Pol Liebgott^{1*}

5 ¹Aix Marseille Univ., Université de Toulon, IRD, CNRS, MIO UM 110, 13288, Marseille, France

6 ²IFREMER, CNRS, Université de Bretagne Occidentale, Laboratoire de Microbiologie des Environnements Extrêmes –
7 UMR6197, Ifremer, Centre de Brest CS10070, Plouzané, France.

8 ³Aix Marseille Univ, CNRS, Centrale Marseille, iSm2, Marseille, France

9 * To whom correspondence may be addressed. Email: pierre-pol.liebgott@mio.osupytheas.fr; Mediterranean Institute
10 of Oceanography, Campus de Luminy, Bâtiment OCEANOMED, 13288 Marseille Cedex 09.

11 <https://orcid.org/0000-0002-2559-1738>

12 **Key-words**

13 Electrotrophy, hyperthermophiles, microbial electrochemical system, deep-sea hydrothermal
14 vent, electrosynthesis

15 **Summary**

16 Deep-sea hydrothermal vents are extreme and complex ecosystems based on a trophic chain. We
17 are still unsure of the first colonizers of these environments and their metabolism, but they are
18 thought to be (hyper)thermophilic autotrophs. Here we investigate whether the electric potential
19 observed across hydrothermal chimneys could serve as an energy source for these first colonizers.
20 Experiments were performed in a two-chamber microbial electrochemical system inoculated with
21 deep-sea hydrothermal chimney samples, with a cathode as sole electron donor, CO₂ as sole
22 carbon source, and three different electron acceptors (nitrate, sulfate, and oxygen). After a few
23 days of culture, all three experiments showed growth of an electrotrophic biofilm consuming
24 directly or indirectly the electrons and producing organic compounds including acetate, glycerol,

25 and pyruvate. The only autotrophs retrieved were members of *Archaeoglobales*, in all three
26 experiments. Various heterotrophic phyla also grew through trophic interactions, with
27 *Thermococcales* in all three experiments and other bacterial groups specific to each electron
28 acceptor. This electrotrophic metabolism as energy source to drive the first microbial colonization
29 of conductive hydrothermal chimneys was discussed.

30 **Introduction**

31 Deep-Sea hydrothermal vents, are geochemical structures housing an extreme ecosystem rich in
32 micro- and macro-organisms. Since their discovery in 1977 (Corliss and Ballard, 1977), they
33 attracted the interest of researcher and, more recently, industries by their singularities. Isolated
34 in the deep ocean, far from the sunlight and subsequent organic substrate, the primal energy
35 sources for the development of this luxuriant biosphere remain elusive in these extreme
36 environments rich in minerals. Since their discovery, many new metabolisms have been identified
37 based on organic or inorganic molecules. However, the driving force sustaining all biodiversity in
38 these environments is thought to be based on chemolithoautotrophy (Alain *et al.*, 2004). Indeed,
39 unlike most ecosystems, deep-sea ecosystems are totally dark and microorganisms have adapted
40 to base their metabolism on lithoautotrophy using inorganic compounds as the energy source to
41 fix inorganic carbon sources. Primary colonizers of deep-sea hydrothermal vents are assumed to
42 be (hyper)thermophilic microbes developing near the hydrothermal fluid, as retrieved in young
43 hydrothermal chimneys. These first colonizers are affiliated to *Archaea*, such as *Archaeoglobales*,
44 *Thermococcales*, *Methanococcales* or *Desulfurococcales*, and to *Bacteria* from ϵ -*proteobacteria*
45 and *Aquificales*. (Huber *et al.*, 2002, 2003; Nercessian *et al.*, 2003; Takai *et al.*, 2004). Recent
46 studies have also shown that hyperthermophilic *Archaea*, which count among the supposed first
47 colonizers, are able to quickly scan and fix onto surfaces to find the best conditions for growth
48 (Wirth *et al.*, 2018). These hyperthermophilic microorganisms would fix inorganic carbon through

49 chemolithoautotrophic types of metabolism, using H₂, H₂S or CH₄ as energy sources and oxidized
50 molecules such as oxygen, sulfur compounds, iron oxide or even nitrate as electron acceptors.
51 However, the discovery of the presence of an abiotic electric current across the chimney walls
52 (Yamamoto *et al.*, 2017) prompted the hypothesis of a new type of microorganisms called
53 eletrotrophs having the capacity to use electrons from the abiotic electric current as an energy
54 source coupled with carbon fixation from CO₂. This metabolism was identified a few years ago on
55 a mesophilic chemolithoautotrophic Fe(II)-oxidizing bacterium, *Acidithiobacillus ferrooxidans*
56 (Ishii *et al.*, 2015). This strain was able to switch its source of energy from diffusible Fe²⁺ ions to
57 direct electron uptake from a polarized electrode. However, this feature has not yet been
58 demonstrated in deep-sea hydrothermal vent environments. Recent studies have shown the
59 exoelectrogenic ability of some hyperthermophilic microorganisms isolated from deep-sea
60 hydrothermal vents, belonging to *Archaeoglobales* and *Thermococcales* (Pillot *et al.*, 2018, 2019;
61 Yilmazel *et al.*, 2018), but no studies have been done on environmental samples potentially
62 harboring electrotrophic communities growing naturally with an electric current as sole energy
63 source.

64 Here, we investigate the potential presence of electrotrophic communities in deep-sea
65 hydrothermal vents capable of using electrons directly or indirectly from the abiotic current. In
66 this purpose, we mimic the conductive surface of the hydrothermal chimney in a cathodic
67 chamber of Microbial Electrochemical Systems (MES) with a polarized cathode to enrich the
68 potential electrotrophic communities inhabiting these extreme environments. The polarized
69 cathode served as the sole energy source, while CO₂ bubbling served as sole carbon source. Three
70 electron acceptors were tested separately, i.e. nitrate, oxygen, and sulfate, to show the influence
71 of an electron acceptor on community taxonomic composition.

72 **Results**

73 **Current consumption from electrotroph enrichments**

74 Hydrothermal vents chimney samples were inoculated in MES filled with sterile mineral medium
75 and incubated at 80°C to enrich electrotrophic communities. In the latter, the electrode served as
76 the sole energy donor (cathode) and sparged CO₂ as carbon source with three different electron
77 acceptors that were tested separately: (i) nitrate, (ii) sulfate and (iii) oxygen. The microbial
78 electrotrophic enrichment was monitored at lowest possible potentials. These potentials were
79 poised at -300mV/SHE in presence of oxygen and -590mV/SHE for both nitrate and sulfate,
80 respectively. For comparison, microbial growth was also monitored without any poised potential
81 during a month in the same conditions of incubation. Interestingly, in the latter condition, no
82 microbial growth occurred, supported by microscope and spectrophotometric observations (data
83 not shown). Moreover, no organic compounds were produced supported by the HPLC and NMR
84 measurements (data not shown).

85 When potential was poised, abiotic controls containing no inoculum displayed constant currents
86 of $\approx 0,016 \text{ A.m}^{-2}$ at -590 mV and $\approx 0,01 \text{ A.m}^{-2}$ at -300 mV/SHE. In both conditions, the potential
87 hydrogen production on the cathode by water electrolysis was quantified and was under the
88 detection threshold of the μGC ($>0.001\%$ of total gas), indicating a theoretical production lower
89 than $34 \mu\text{M day}^{-1}$ (data not shown), similar as previously reported at 25°C (Marshall *et al.*, 2013).
90 In comparison, experiments with the chimney sample showed current consumptions increasing
91 shortly after inoculation (Fig. 1). Indeed, when subtracting abiotic current, the current
92 consumptions reached a stabilized maximum of 0.36 A.m^{-2} on oxygen, 0.72 A.m^{-2} on nitrate, and
93 up to 1.83 A.m^{-2} on sulfate corresponding therefore to an increase of 36, 45 and 114-fold
94 compared to abiotic current, respectively. MES were autoclaved afterwards displaying decreased
95 currents that were similar to the values of abiotic controls with a stabilized current around $\approx 0,021$
96 A.m^{-2} .

97 At the end of monitoring of current consumption, CycloVoltamograms (CV) were performed to
98 study reactions of oxidation and reduction that could occur in MES (Supporting Information Fig.

99 S1A). A first peak of reduction is observed at -0.295, -0.293 and -0.217 V vs SHE in presence of
100 nitrate, sulfate and oxygen as electron acceptor, respectively (Fig. S1B). A second peak is observed
101 at -0.639 and -0.502 V vs SHE on nitrate and sulfate, respectively. No redox peaks are detected in
102 the abiotic controls and freshly inoculated MES, hence indicating a lack of electron shuttles
103 brought with the inoculum (Fig. S1A).

104 **Organic compounds production in liquid media**

105 During enrichment of the electrotrophic communities, the production of organic compounds was
106 monitored in liquid media (Fig. 1). Interestingly, the glycerol, the pyruvate, and the acetate were
107 the dominant products released in all experiment runs. Glycerol increased slowly throughout the
108 experiments to reach a maximum of 0.47 mM on sulfate (day 11), 1.32 mM on oxygen (day 12)
109 and 2.32 mM on nitrate (day 19). Acetate accumulated in the medium to reach 0.33 mM on
110 oxygen (day 7), 0.75 mM on sulfate (day 13) and 1.40 mM on nitrate (day 19). Pyruvate was
111 produced after a few days of culture with an exponential curve, reaching a maximum of 1.32 mM
112 on oxygen (day 12), 2.39 mM on nitrate (day 9), and 3.94 mM on sulfate (day 11). Pyruvate varied,
113 afterwards, due probably to microbial consumption or thermal degradation... Coulombic
114 efficiency calculated on the last day of the experiment (Fig. 2) showed up to 71% (on nitrate),
115 89% (on oxygen) and 90% (on sulfate) of electrons consumed were converted to organic
116 compounds and released into the liquid media .The rest represents the share of electrons
117 retained in not accumulated compounds (Table S1) and in the organic matter constituting the
118 cells of the electrotrophic communities (estimated by qPCR to total between 10^8 to 10^{10} 16S rRNA
119 gene copies per MES; Supporting Information Fig. S2).

120 **Biodiversity of electrotrophic communities on different electron acceptors**

121 Once current consumption reached a stabilized maximum, DNAs from the biofilm and from
122 planktonic cells in culture media were extracted and sequenced on the V4 region of the 16S rRNA

123 to study relative abundance of the biodiversity. Fig. 3 reports the taxonomic affiliation of the
124 OTUs obtained. The chimney fragment inoculum showed a rich biodiversity (Shannon index at
125 5.29 and Pielou's index at 0.69), with 208 OTUs mainly affiliated to *Bacteria* (99.49% vs 0.51% of
126 *Archaea*) and more particularly to *Proteobacteria* from *Vibrionales* (34.8%), miscellaneous rare
127 *Proteobacteria* (>33%), *Campylobacterales* (8.3%), *Thermales* (7.1%), *Aquificales* (5.62%), and
128 *Rhodobacterales* (5.1%).

129 Enrichments in MES showed less biodiversity on cathodes and liquid media, suggesting the
130 selective development of functional communities. The Shannon index values were 3.1 and 1.9 on
131 nitrate, 1.7 and 1.9 on sulfate, and 4.1 and 4.2 on oxygen, with fewer OTUs associated to 72 and
132 68 OTUs on nitrate, 39 and 53 on sulfate, and 94 and 102 on oxygen, on electrodes and liquid
133 media, respectively. The taxonomic composition of these communities showed a larger
134 proportion of *Archaea*, with 51% and 41.6% on nitrate, 96.8% and 96.3% on sulfate, and 7.6% and
135 3.4% on oxygen on the electrodes and liquid media, respectively. In presence of each electron
136 acceptor, the archaeal population on the electrode was mainly composed of *Archaeoglobales* and
137 *Thermococcales* at different relative abundances. The latter were present at 6.7% and 28.2% on
138 nitrate to 65.8% and 28.6% on sulfate and 3.8% and 3.6% on oxygen, respectively. Equivalent
139 proportions of *Archaeoglobales* and *Thermococcales* were retrieved in liquid media, at 1.0% and
140 2.5% on nitrate, 65.8% and 29.6% on sulfate and 0.3% and 2.7% on oxygen, respectively (Fig. 3).

141 The MiSeq Illumina results served to study only 290 bp of 16S rRNA and thus to affiliate
142 microorganisms confirmed at family level, but they can also provide some information on the
143 enriched genera. In an effort to obtain more information on the probable *Archaeoglobales* and
144 *Thermococcales* genus, we attempted a species-level identification through phylogenetic analysis.
145 The results are presented in Fig. 4 as a Maximum Likelihood phylogenetic tree. The dominant
146 OTUs on sulfate and oxygen were closest to *Ferroglobus placidus* and *Archeoglobus fulgidus*
147 97.61% whereas the dominant OTU on nitrate was affiliated to *Geoglobus ahangari* with an

148 identity of 98.63% of identity. The remaining part of the biodiversity was specific to each electron
149 acceptor used. Enrichment on nitrate showed 13.8% and 28% of *Desulfurococcales* and 46.2% and
150 56.5% of *Thermales* on the electrode and in liquid media, respectively. Among *Thermales* that
151 developed on the electrode, 30% were represented by a new taxon (OTU 14 in Fig. 4 and S3)
152 whose closest cultured species was *Vulcanithermus mediatlanticus* (90% similarity). On sulfate,
153 the remaining biodiversity represented less than 4% of the population but was mainly
154 represented by two particular OTUs. The first OTU, accounting for up to 2.4% and 0.8% of the
155 total population on the electrode and liquid media, respectively, was affiliated to a new
156 *Euryarchaeota* (OTU 10 in Fig. 4 and S3) whose closest cultured match was *Methanothermus*
157 *fervidus* strain DSM 2088, at 86% similarity. The second OTU accounted for 2.0% and 1.9% of the
158 biodiversity on the electrode and liquid media, respectively, and was affiliated to the new
159 *Deinococcales* (OTU 14 in Fig. 4 and S3) species, found mostly on the electrode in nitrate
160 enrichment. In the enrichment on oxygen, the communities are dominated by 36.6% and 30.2% of
161 *Pseudomonadales* (*Pseudomonas* sp.), 14% and 42.6% of *Bacillales* (*Bacillus* and *Geobacillus* sp.),
162 21.3% and 7.41% of *Vibrionales* (*Photobacterium* sp.), and 9.8% and 5.1% of *Actinomycetales*
163 (spread across 9 species) on the electrode and in liquid media, respectively, with the rest spread
164 across *Proteobacteria* orders.

165 The clustering of the dominant OTUs (at a threshold of 0.05% of total sequences) obtained
166 previously on the chimney sample and enrichments in MES showed a clear differentiation of
167 communities retrieved in each sample (Supporting Information Fig. S3). The Pearson method on
168 OTU distribution produced four clusters, one corresponding to the inoculum and the three others
169 to each electron acceptor. Indeed, only two OTUs (OTU 4 and 36) were clearly shared between
170 two different communities, one affiliated to *Thermococcus* spp. on nitrate and sulfate and one to
171 *Ralstonia* sp. on the chimney sample and on nitrate. It is surprising to observe a recurrence of this
172 last OTU which could be a contaminant specific to the extraction kit used (Salter *et al.*, 2014). The

173 other 50 dominant OTUs were specific to one community, with 21 OTUs on oxygen, 4 on sulfate, 8
174 on nitrate, and 17 on the chimney sample. The electrotrophic communities, colonizing the
175 cathode, were therefore different depending on electron acceptor used and their concentration
176 was too low to be detected in the chimney sample.

177 **Discussion**

178 **Archaeoglobales as systematic (electro)lithoautotrophs of the community**

179 Herein, we evidenced the development of a microbial electrotrophic communities and metabolic
180 activity supported by current consumption (Fig.1), product production (Fig. 2), and qPCRs (Fig. S2)
181 suggesting that growth did occur from energy supplied by the cathode. The mechanism of energy
182 uptake from electrode is discussed since the discovery of biofilms growing on cathode, and little is
183 known, unlike electron transfer mechanism on anode. The two main hypotheses are the use of
184 similar direct electron transfer pathway as on the anode, or the use of molecular H₂, produced by
185 water electrolysis, as electron mediator to the cell. In both cases, our study is the first to show the
186 possibility of growth of biofilm from environments harboring natural electric current in absence of
187 organic substrates. To discuss further on the putative mechanism, it is necessary to have a look on
188 the conditions for water electrolysis. The potential for water reduction into hydrogen at 80°C, pH7,
189 1 atm was calculated at -0.490 V vs SHE in pure water. The real operational reduction potentials is
190 expected to be much more lower than the theoretical value due to internal resistances (from
191 electrical connections, electrolyte, ionic membrane etc.) (Lim *et al.*, 2017). Moreover,
192 overpotentials are expected with carbon electrodes. The decrease of this potential explains the
193 absence of hydrogen measured in our conditions. A screening of potential in abiotic conditions
194 confirmed the increase of current consumption and H₂ production only at potential lower of -0.6V
195 vs SHE (Fig S1) Moreover several pieces of evidence indicate that direct electron transfer may have
196 mainly participated in the development of biofilms: the growth of the similar dependent sulfate
197 biodiversity with the cathode poised at -300 mV vs SHE (Supporting Information Fig. S4) without H₂

198 production, the expression of catalytic waves observed by CV with midpoint potentials between -
199 0.217 V to -0.639 V and the lack of similar peaks with abiotic or fresh inoculated media (Supporting
200 Information Fig. S1), biofilm formation on the electrode (as on nitrate, Supporting Information Fig.
201 S5), delayed production of glycerol, pyruvate and acetate (Fig. 1) fixing between 267 to 1596
202 Coulombs.day⁻¹ (organic consumption deduced), and the recovery of electrons in all three products
203 (Fig. 2), that largely exceeds the maximum theoretical abiotic generation of hydrogen (~3 C.day⁻¹)
204 by 90 to 530-fold. Thus, we can assume that the biofilm growth was largely ensured by a significant
205 part of a direct transfer of electrons from the cathode demonstrating the presence of
206 electrolithoautotroph microorganisms.

207 Taxonomic analysis of the enriched microbial communities at the end of the experiments showed
208 the systematic presence on cathodes of *Archaeoglobales* (Fig. 3 and S3), whatever the electron
209 acceptors used. The species belonging to *Archaeoglobales* order were the only enriched species in
210 all conditions and the only known to have an autotrophic metabolism (except for *Archaeoglobus*
211 *profundus* and *A. infectus* which are obligate heterotrophs). The *Archaeoglobales* order is
212 composed of three genera: *Archaeoglobus*, *Geoglobus*, and *Ferroglobus*. All are hyperthermophilic
213 obligate anaerobes with diverse metabolisms, including heterotrophy or chemolithoautotrophy.
214 Terminal electron acceptors used by this order include sulfate, nitrate, poorly crystalline Fe (III)
215 oxide, or sulfur oxyanions (Brileya and Reysenbach, 2014). Autotrophic growth in the
216 *Archaeoglobales* order is ensured mainly through H₂ as energy source and requires both branches
217 of the reductive acetyl-CoA/Wood-Ljungdahl pathway for CO₂ fixation (Vorholt *et al.*, 1997).
218 Moreover, *Archaeoglobus fulgidus* has been recently shown to grow on iron by directly snatching
219 electrons under carbon starvation during corrosion process (Jia *et al.*, 2018). Furthermore,
220 *Ferroglobus* and *Geoglobus* species were shown to be exoelectrogens in pure culture in a microbial
221 electrosynthesis cell (Yilmazel *et al.*, 2018) and were enriched during a study within a microbial
222 electrolysis cell (Pillot *et al.*, 2018, 2019). Interestingly, some studies have shown that *Geobacter*

223 species are capable of bidirectional electron transfer using the same mechanism (Pous *et al.*, 2016).
224 Hence, *Archaeoglobales* that have been shown already as exoelectrogens (Yilmazel *et al.*, 2018)
225 could also be electrotrophy. It is not known how Archaea carry out exogenous electron transfer. As
226 previously discussed, the absence of H₂ production and the increasing current consumptions over
227 time suggest direct electron uptake from members of the communities developing on the
228 electrode, as for *Acidithiobacillus ferroxidans* (Ishii *et al.*, 2015). Moreover, the qPCR (Supporting
229 Information Fig. S2) and MiSeq data (Fig. 3) highlighted a strong correlation between current
230 consumption and density of *Archaeoglobales* on the electrode ($R^2=0.962$). In the condition with
231 sulfate as electron acceptor, the proportion of *Archaeoglobales* represented 65.8% of total
232 biodiversity providing 1.83 A.m⁻² of current consumption, compared to only 6.7% in the nitrate
233 condition and 3.8% in the oxygen condition for 0.72 and 0.36 A.m⁻² of current consumption,
234 respectively. Moreover, the majority of OTUs were affiliated to three *Archaeoglobaceae* genera,
235 mainly *Archaeoglobus* spp. and *Ferroglobus* spp. on sulfate and oxygen and *Geoglobus* sp. on
236 nitrate. Some *Archaeoglobus* are known to show anaerobic sulfate-reducing metabolism while
237 *Ferroglobus* spp. are not. *Geoglobus* sp. has never been described to perform nitrate reduction so
238 far, but it does harbor genes of nitrate- and nitrite-reductase-like proteins (Manzella *et al.*, 2015).
239 The OTUs were related to some *Archaeoglobales* strain with 95-98% identities. Thus, we assume
240 that in our conditions, new specific electrotrophic metabolisms or new electrolithoautotrophic
241 *Archaeoglobaceae* species were enriched on the cathode. Moreover, a member of a new
242 phylogenetic group of *Archaea* was enriched up to 2.4% of total biodiversity on sulfate (OTU10 in
243 Fig. 4). While its metabolism is still unknown, we suggest that isolation of this electrotrophic
244 archaea in MES could enable the identification of a new archaeal phylogenetic group based on
245 electrotrophy.

246 The growth of *Archaeoglobales* species in presence of oxygen is a surprising finding.

247 *Archaeoglobales* have a strictly anaerobic metabolism, and the reductive acetyl-CoA pathway is

248 very sensitive to the presence of oxygen (Fuchs, 2011). This can be firstly explained by the low
249 solubility of oxygen at 80°C combined with the electrochemically oxygen reduction on electrode
250 in controls (data not shown). It hence results in an low oxygen or oxygen-free environment within
251 the carbon cloth mesh for anaerobic development of microorganisms into a protective biofilm
252 (Hamilton, 1987). This observation was also supported by the near absence of *Archaeoglobales* in
253 the liquid media (Fig. 3). In absence of other electron acceptors, some *Archaeoglobales* perform
254 carboxydrotrophic metabolism to grow from CO, as demonstrated for *Archaeoglobus fulgidus*
255 (Sokolova and Lebedinsky, 2013; Hocking *et al.*, 2015). This fermentative CO metabolism leads to
256 the production of acetate and transient accumulation of formate via the Wood-Ljungdahl
257 pathway, but no net ATP is really produced (Henstra *et al.*, 2007). The energy conservation
258 through this metabolism in *Archaeoglobus fulgidus* is still poorly understood (Hocking *et al.*,
259 2015). A second hypothesis concerns direct interspecies electron transfer (DIET) (Kato *et al.*,
260 2012; Lovley, 2017), with *Archaeoglobales* transferring electrons to another microorganism as an
261 electron acceptor. Research into DIET is in its early stages, and further investigations are required
262 to better understand the diversity of microorganisms and the mechanism of carbon and electron
263 flows in anaerobic environments (Lovley, 2017) such as hydrothermal ecosystems.

264 **Electrosynthesis of organic compounds**

265 The pyruvate, the glycerol and the acetate accumulated, while another set of compounds that
266 appear transiently were essentially detectable in the first few days of biofilm growth (Supporting
267 Information Table S1). They included amino acids (threonine, alanine) and volatile fatty acids
268 (formate, succinate, lactate, acetoacetate, 3-hydroxyisovalerate) whose concentrations did not
269 exceed one micromole. Despite their thermostability, this transient production suggests they
270 were used by microbial communities developing on the electrode in interaction with the primary
271 producers during enrichment.

272 On the other hand, in presence of nitrate, sulfate and oxygen as electron acceptors, the liquid
273 media accumulated three main organic products acetate, glycerol, and pyruvate (Fig. 1).
274 Coulombic efficiency calculations (Fig. 2) showed that redox levels of the carbon-products
275 represented 71%–90% of electrons consumed, and only about 10%–30% of net electrons
276 consumed by electrotroths during growth was used directly for biomass or transferred to an
277 electron acceptor. This concurs with the energy yield from the Wood-Ljungdahl pathway of
278 *Archaeoglobales*, with only 5% of carbon flux directed to the production of biomass and the other
279 95% diverted to the production of small organic end-products excreted from the cell (Fast and
280 Papoutsakis, 2012).

281 However, the production of pyruvate and glycerol warrants further analysis. Pyruvate is normally
282 a central intermediate of CO₂ uptake by the reducing route of the acetyl-CoA/WL pathway (Berg
283 *et al.*, 2010). It can be used to drive the anabolic reactions needed for biosynthesis of cellular
284 constituents. Theoretically, the only explanation for improved production and accumulation of
285 pyruvate (up to 5 mM in the liquid media of sulfate experiment) would be that pyruvate-using
286 enzymes were inhibited or that pyruvate influx exceeded its conversion rate. Here we could
287 suggest that in-cell electron over-feeding at the cathode leads to significant production of
288 pyruvate. Indeed, in a physiological context, the production of pyruvate from acetyl-CoA via
289 pyruvate synthase requires the oxidation of reduced ferredoxins for CO₂ fixation (Furdui and
290 Ragsdale, 2000). The continuous electron uptake from the cathode would lead to a significant
291 reduction in electron carriers (including ferredoxins, flavins, cytochromes, and/or nicotinamides),
292 thus forcing the electrotrophic microbial community to produce pyruvate as a redox sink.

293 In the same context of pyruvate production, glycerol is produced by reduction of
294 dihydroxyacetone phosphate a glycolytic intermediate, to glycerol 3-phosphate (G3P) followed by
295 dephosphorylation of G3P to glycerol. In some yeasts, glycerol production is essential for
296 osmoadaptation but equally for regulating the NADH surplus during anaerobic growth (Björkqvist

297 *et al.*, 1997). A similar mechanism may operate in our conditions for the probable excess of NADH
298 pool due to the electrode poised at -590 mV vs SHE, which would explain the accumulation of
299 glycerol found in our experiments.

300 In an ecophysiological context, a similar pyruvate and glycerol production could occur on
301 hydrothermal chimney walls into which electric current propagates (Yamamoto *et al.*, 2017). The
302 electrotoph biofilms would continually receive electrons, leading to the excess of intracellular
303 reducing power that would be counterbalanced by the overproduction of glycerol and pyruvate.
304 Moreover, glycerol is an essential compound in the synthesis of membrane lipids in *Archaea* and
305 probably also in biofilm formation and osmoadaptability (Desai *et al.*, 2013; Shemesh and Chai,
306 2013). Pyruvate unites several key metabolic processes, such as its conversion into carbohydrates,
307 fatty acids or some amino acids. Furthermore, these products can serve as carbon and energy
308 sources for heterotrophic microorganisms or for fermentation. In our experiments, pyruvate and
309 glycerol concentrations varied over time, suggesting they were being consumed by heterotrophic
310 microorganisms. Acetate production would thus result from the fermentation of pyruvate or
311 other compounds produced by electrotophic *Archaeoglobales*.

312 **Enrichment of rich heterotrophic biodiversity from electrotophic Archaeoglobales** 313 **community**

314 During our enrichment experiments, the development of effective and specific biodiversity was
315 dependent on the electron acceptors used (Fig. 3). Heatmap analyses (Supporting Information Fig.
316 3) showed four distinct communities for the three electron acceptors and the initial inoculum. Thus,
317 at the lower taxonomic level of the biodiversity analysis, most OTUs are not shared between each
318 enrichment, except for one OTU of *Thermococcales* that was shared between the nitrate and sulfate
319 experiments. This suggests a real specificity of the communities and a specific evolution or
320 adaptation of the members of the shared phyla to the different electron acceptors available in the
321 environment. However, the various enrichments also showed the presence of *Thermococcales*

322 regardless of the electron acceptors used, thus demonstrating a strong interaction between
323 *Thermococcales*, heterotrophs, and *Archaeoglobales*, the only autotrophs. In a previous study,
324 enrichments on the anode of a microbial electrolysis cell showed a similar tendency, with
325 *Archaeoglobales* strongly correlated to *Thermococcales* (Pillot *et al.*, 2018, 2019). Moreover,
326 members of these two groups have frequently been found together in various hydrothermal sites
327 on the surface of the Earth (Corre *et al.*, 2001; Nercessian *et al.*, 2003; Takai *et al.*, 2004; Jaeschke
328 *et al.*, 2012), where they are considered as potential primary colonizers of their environments (33–
329 36). This could point to a co-evolution and metabolic adaptation of these microorganisms to their
330 unstable environmental conditions in hydrothermal settings. After *Thermococcales*, the rest of the
331 heterotrophic biodiversity was specific to each electron acceptor.

332 On nitrate, two additional phylogenetic groups were retrieved: *Desulfurococcales* and *Thermales*.
333 OTUs of *Desulfurococcales* are mainly affiliated to *Thermodiscus* or *Aeropyrum* species, which are
334 hyperthermophilic and heterotrophic *Crenarchaeota* growing by fermentation of complex organic
335 compounds or sulfur/oxygen reduction (Huber and Stetter, 2015).

336 Concerning *Thermales*, a new taxon was enriched on cathode and only affiliated with 90 %
337 similarity to *Vulcanithermus mediatlanticus*. On sulfate, beside the large majority of
338 *Archaeoglobales* and *Thermococcales* (up to 94%–96%), this new taxon of *Thermales* (OTU 14, Fig.
339 S3) has also been enriched on the cathode, representing 2% of total biodiversity. *Thermales* are
340 thermophilic (30°C–80°C) and heterotrophic bacteria whose only four genera (*Marinithermus*,
341 *Oceanithermus*, *Rhabdothermus*, and *Vulcanithermus*) are all retrieved in marine hydrothermal
342 systems. They are known to be aerobic or microaerophilic. Some strains grow anaerobically with
343 several inorganic electron acceptors such as nitrate, nitrite, Fe (III) and elemental sulfur
344 (Albuquerque and Costa, 2014). All of the species *Thermales* can utilize the pyruvate as carbon
345 and energy source. The produced pyruvate would be a substrate of choice for this new taxon
346 which would use the sulfate and nitrate as electron acceptors.

347 *Pseudomonadales* and *Bacillales* were found in the oxygen experiment. Most *Pseudomonas* are
348 known to be aerobic and mesophilic bacteria, with a few thermophilic species, including the
349 autotrophic *Pseudomonas thermocarboxydovorans* that grows at up to 65°C (Lyons *et al.*, 1984;
350 Palleroni, 2015). There have already been reports of mesophilic *Pseudomonas* species growing in
351 thermophilic conditions in composting environments (Droffner *et al.*, 1995). Moreover, some
352 *Pseudomonas* sp. are known to be electroactive in microbial fuel cells, through long-distance
353 extracellular electron transport (Shen *et al.*, 2014; Maruthupandy *et al.*, 2015; Lai *et al.*, 2016),
354 and were dominant on the cathodes of a benthic microbial fuel cell on a deep-ocean cold seep
355 (Reimers *et al.*, 2006). In *Bacillales*, the *Geobacillus* spp. and some *Bacillus* sp. are known to be
356 mainly (hyper)thermophilic aerobic and heterotrophic *Firmicutes* (Vos, 2015).

357 **Hydrothermal electric current: a new energy source for the development of primary** 358 **producers**

359 The presence of so many heterotrophs in an initially autotrophic condition points to the
360 hypothesis of a trophic relationship inside the electrotrophic community (Fig. 5). This suggests
361 that the only autotrophs retrieved in all communities, the *Archaeoglobales*, might be the first
362 colonizer of the electrode, using CO₂ as carbon source and cathode as energy source. Studies have
363 shown how modeling and field observations can be usefully combined to describe the relationship
364 between chemical energy conditions and metabolic interactions within microbial communities
365 (Lin *et al.*, 2016; Dahle *et al.*, 2018). However, the models predicted low abundances of
366 *Archaeoglobales* (<0.04%) whereas on-field detection found abundances of more than 40% in the
367 inner section of the studied hydrothermal chimney (Dahle *et al.*, 2018). Indeed, in these models,
368 the predicted H₂ concentration, based on observations, would be too low to support the growth
369 of hydrogenotrophic or methanogenic species (Lin *et al.*, 2016). The authors concluded on a
370 probable H₂ syntrophy, with hydrogen being produced by heterotrophic microorganisms such as
371 fermentative *Thermococcales* species. Our study is the first evidence of the development of

372 hyperthermophilic electrotrophic/heterotrophic communities directly enriched from the natural
373 environment known to harbor natural electric current as a potential energy source. We can thus
374 conclude that this kind of electrolithoautotrophic metabolism is highly likely in deep-sea
375 hydrothermal ecosystems, which raises the question of the importance of this metabolism in the
376 primary colonization of hydrothermal vents. The hydrothermal electric current could make up for
377 the lack of H₂ normally needed to sustain the growth of hydrogenotrophic microorganisms.
378 Indeed, the constant electron supply on the surface of a conductive chimney allows a new energy
379 source and long-range transfer between the electron donor (represented here by reduced
380 molecules such as H₂S electrochemically oxidized on the inner surface of the chimney wall) and
381 the electron acceptor (O₂, sulfur compounds, nitrate, metals) present all over the external surface
382 of the chimney. This electrical current would thus allow primary colonizers to grow not just on all
383 the surface but also in the chimney structure. These primary colonizers would release organic
384 compounds used by the heterotrophic community for growth, as observed with the successive
385 production and consumption of organic compounds in our experiments. Moreover, migrating out
386 to larger potential growth surface would help to meet a wider range of physiological conditions
387 through pH, temperature and oxidoreduction gradients. This allows a wider diversity of growth
388 patterns than through chemolithoautotrophy, which is restricted to unstable and limited contact
389 zones between reduced compounds (H₂, H₂S) in the hydrothermal fluid and electron acceptors
390 around the hydrothermal chimneys, often precipitating together.

391 **Conclusion**

392 Taken together, the results found in this study converge into evidence of the ability of indigenous
393 microorganisms from deep hydrothermal vents to grow using electric current and CO₂. This ability
394 seems to be spread across diverse phylogenetic groups and to be coupled with diverse electron
395 acceptors. Through their electro-litho-auto-trophic metabolism, *Archaeoglobaceae* strains
396 produce and release organic compounds into their close environment, allowing the growth of

397 heterotrophic microorganisms, and ultimately enabling more and more diversity to develop over
398 time. This metabolism could be one of the primary energies for the colonization of deep-sea
399 hydrothermal chimneys and the development of a complex trophic network driving sustainable
400 biodiversity. A similar mechanism could have occurred during the Hadean, allowing the
401 emergence of life in hydrothermal environments by constant electron influx to the first proto-
402 cells.

403 **Experimental procedures**

404 **Sample collection and preparation**

405 A hydrothermal chimney sample was collected on the acidic and iron-rich Capelinhos site on the
406 Lucky Strike hydrothermal field (37°17.0'N, MAR) during the MoMARSat cruise in 2014
407 (<http://dx.doi.org/10.17600/14000300>) led by IFREMER (France) onboard R/V *Pourquoi Pas?*
408 (Sarradin and Cannat, 2014). The sample (PL583-8) was collected by breaking off a piece of a high-
409 temperature active black smoker using the submersible's robotic arm, and bringing it back to the
410 surface in a decontaminated insulated box (<http://video.ifremer.fr/video?id=9415>). Onboard,
411 chimney fragments were anaerobically crushed in an anaerobic chamber under H₂:N₂ (2.5:97.5)
412 atmosphere (La Calhene, France), placed in flasks under anaerobic conditions (anoxic seawater at
413 pH 7 with 0.5 mg L⁻¹ of Na₂S and N₂:H₂:CO₂ (90:5:5) gas atmosphere), and stored at 4°C.
414 Prior to our experiments, pieces of the hydrothermal chimney were removed from the sulfidic
415 seawater flask, crushed with a sterile mortar and pestle in an anaerobic chamber (Coy
416 Laboratories, Grass Lake, MI), and distributed into anaerobic tubes for use in the various
417 experiments.

418 **Electrotrophic enrichment on nitrate, sulfate, and oxygen**

419 MES were filled with 1.5 L of an amended sterile mineral medium as previously described (Pillot
420 *et al.*, 2018) without yeast extract, and set at 80°C and pH 6.0 throughout on-platform monitoring.
421 The electrode (cathode) composed of 20 cm² of carbon cloth was poised at the lowest potential

422 before initiation of abiotic current consumption (Supporting Information Fig S6) using SP-240
423 potentiostats and EC-Lab software (BioLogic, France). We thus used a potential of -590 mV vs(in
424 the nitrate and sulfate experiments and -300 mV vs SHE in the oxygen experiment. A similar
425 experiment at -300 mV vs SHE has been initiated in presence of sulfate (see SI Fig. S4) to confirm
426 the growth of electrolithoautotroph microorganisms without any H₂ production possible. The
427 electrode poised as cathode served as the sole electron donor for electrotrroph growth. For the
428 nitrate experiment, one system was supplemented with 4 mM of sodium nitrate. For the sulfate
429 experiment, a second system was supplemented with 10 mM of sodium sulfate, and the cathodic
430 chambers were sparged with N₂:CO₂ (90:10, 100 mL/min). For the oxygen experiment, a third
431 system was sparged with N₂:CO₂:O₂ (80:10:10, 100 mL/min) with initially 10% oxygen as electron
432 acceptor. All three systems were inoculated with 8 g of the crushed chimney (~0.5% (w/v)).
433 Current consumption was monitored via the chronoamperometry method with current density
434 and readings were taken every 10 s. An abiotic control without inoculation showed no current
435 consumption during the same experiment period. CycloVoltammograms (scan rate: 20 mV/s)
436 were analyzed using QSoas software (version 2.1). Coulombic efficiencies where calculates with
437 the following equation:

$$438 \quad CE (\%) = \frac{F \cdot n_e \cdot \Delta[P] \cdot V_{\text{catholyte}}}{\int_{t_0}^t I(t) \cdot dt} \cdot 100$$

439 I(t): current consumed between t₀ and t (A)

440 F: Faraday constant

441 n_e: number of moles of electrons presents per mole of product (mol)

442 Δ[P]: variation of the concentration of organic product between t₀ and t (mol.L⁻¹)

443 V_{catholyte}: volume of catholyte (L)

444 **Identification and quantification of organic compound production**

445 To identify and quantify the production of organic compounds from the biofilm, samples of liquid
446 media were collected at the beginning and at the end of the experiment and analyzed by ^1H NMR
447 spectroscopy. For this, 400 μL of each culture medium, were added to 200 μL of PBS solution
448 prepared in D_2O (NaCl, 140 mM; KCl, 2.7 mM; KH_2PO_4 , 1.5 mM; Na_2HPO_4 , 8.1 mM, pH 7.4)
449 supplemented with 0.5 mmol L^{-1} of trimethylsilylpropionic acid- d_4 (TSP) as NMR reference. All the
450 1D ^1H NMR experiments were carried out at 300 K on a Bruker Avance spectrometer (Bruker,
451 BioSpin Corporation, France) operating at 600 MHz for the ^1H frequency and equipped with a 5-
452 mm BBFO probe.

453 Spectra were recorded using the 1D nuclear Overhauser effect spectroscopy pulse sequence (Trd-
454 $90^\circ\text{-T}_1\text{-}90^\circ\text{-tm-}90^\circ\text{-Taq}$) with a relaxation delay (Trd) of 12.5 s, a mixing time (tm) of 100 ms, and a
455 T_1 of 4 μs . The sequence enables optimal suppression of the water signal that dominates the
456 spectrum. We collected 128 free induction decays (FID) of 65,536 datapoints using a spectral
457 width of 12 kHz and an acquisition time of 2.72 s. For all spectra, FIDs were multiplied by an
458 exponential weighting function corresponding to a line broadening of 0.3 Hz and zero-filled before
459 Fourier transformation. NMR spectra were manually phased using Topspin 3.5 software (Bruker
460 Biospin Corporation, France) and automatically baseline-corrected and referenced to the TSP
461 signal ($\delta = -0.015$ ppm) using Chenomx NMR suite v7.5 software (Chenomx Inc., Canada). A 0.3 Hz
462 line-broadening apodization was applied prior to spectral analysis, and $^1\text{H}\text{-}^1\text{H}$ TOCSY (Bax and
463 Davis, 1985) and $^1\text{H}\text{-}^{13}\text{C}$ HSQC (Schleucher *et al.*, 1994) experiments were recorded on selected
464 samples to identify the detected metabolites. Quantification of identified metabolites was done
465 using Chenomx NMR suite v7.5 software (Chenomx Inc., Canada) using the TSP signal as the
466 internal standard.

467 **Biodiversity analysis**

468 Taxonomic affiliation was carried out according to (Zhang *et al.*, 2016). DNA was extracted from 1
469 g of the crushed chimney and, at the end of each culture period, from scrapings of half of the WE

470 and from centrifuged pellets of 50 mL of spent media. The DNA extraction was carried out using
471 the MoBio PowerSoil DNA isolation kit (Carlsbad, CA). The V4 region of the 16S rRNA gene was
472 amplified using the universal primers 515F (5'-GTG CCA GCM GCC GCG GTA A-3') and 806R (5'-
473 GGA CTA CNN GGG TAT CTA AT-3') (Bates *et al.*, 2011) with Taq&Load MasterMix (Promega). PCR
474 reactions, qPCR, amplicon sequencing and taxonomic affiliation were carried as previously
475 described (Pillot *et al.*, 2018). The qPCR results were expressed in copies number of 16s rRNA
476 gene per gram of crushed chimney, per milliliter of liquid media or per cm² of surface of the
477 electrode. To analyze alpha diversity, the OTU tables were rarefied to a sampling depth of 9410
478 sequences per library, and three metrics were calculated: the richness component, represented
479 by number of OTUs observed, the Shannon index, representing total biodiversity, and the
480 evenness index (Pielou's index), which measures distribution of individuals within species
481 independently of species richness. Rarefaction curves (Supporting Information Fig. S7) for each
482 enrichment approached an asymptote, suggesting that the sequencing depths were sufficient to
483 capture overall microbial diversity in the studied samples. The phylogenetic tree was obtained
484 with MEGA software v10.0.5 with the MUSCLE clustering algorithm and the Maximum Likelihood
485 Tree Test with a Bootstrap method (2500 replications). The heatmap was obtained using RStudio
486 software v3. The raw sequences for all samples can be found in the European Nucleotide Archive
487 (accession number: PRJEB35427).

488 **Acknowledgments**

489 This work received financial support from the CNRS-sponsored national interdisciplinary research
490 program (PEPS-ExoMod 2016). The authors thank Céline Rommevaux and Françoise Lesongeur for
491 taking samples during the MOMARSAT 2014 cruise, the MIM platform (MIO, France) for providing
492 access to their confocal microscopy facility, and the GeT-PlaGe platform (GenoToul, France) for
493 help with DNA sequencing. The project leading to this publication received European FEDER
494 funding under project "1166-39417. The authors declare no conflicts of interest.

496 References

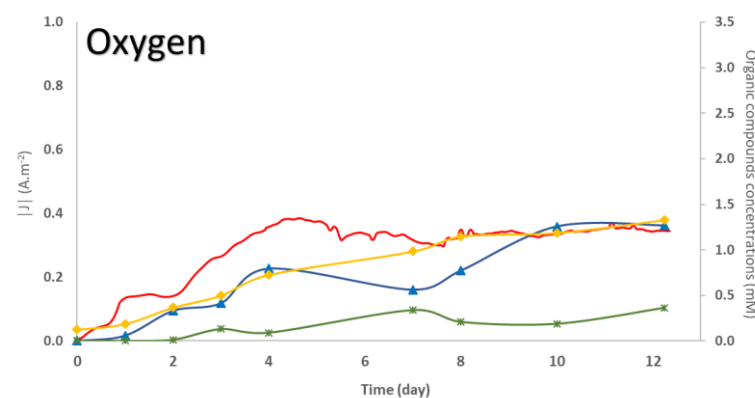
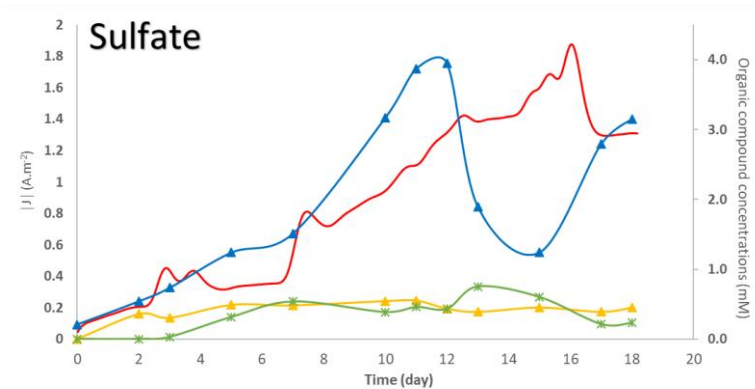
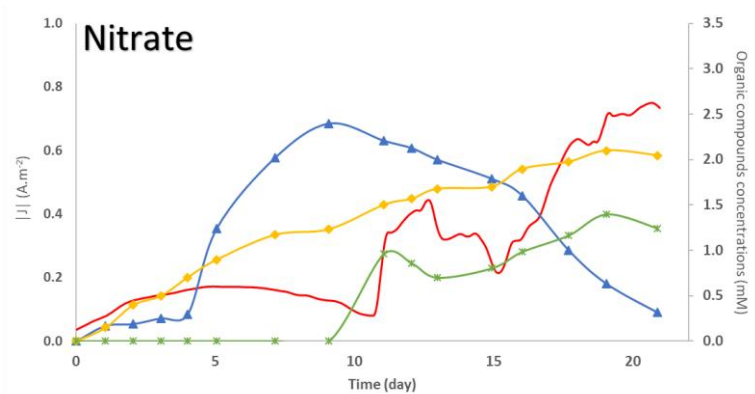
- 497 Alain, K., Zbinden, M., Bris, N.L., Lesongeur, F., Quérellou, J., Gaill, F., and Cambon-Bonavita,
498 M.-A. (2004) Early steps in microbial colonization processes at deep-sea hydrothermal
499 vents. *Environ Microbiol* **6**: 227–241.
- 500 Albuquerque, L. and Costa, M.S. da (2014) The Family *Thermaceae*. In *The Prokaryotes*. Springer,
501 Berlin, Heidelberg, pp. 955–987.
- 502 Bates, S.T., Berg-Lyons, D., Caporaso, J.G., Walters, W.A., Knight, R., and Fierer, N. (2011)
503 Examining the global distribution of dominant archaeal populations in soil. *ISME J* **5**: 908–
504 917.
- 505 Bax, A. and Davis, D.G. (1985) MLEV-17-based two-dimensional homonuclear magnetization
506 transfer spectroscopy. *J Magn Reson* **1969** **65**: 355–360.
- 507 Berg, I.A., Kockelkorn, D., Ramos-Vera, W.H., Say, R.F., Zarzycki, J., Hügler, M., et al. (2010)
508 Autotrophic carbon fixation in archaea. *Nat Rev Microbiol* **8**: 447–460.
- 509 Björkqvist, S., Ansell, R., Adler, L., and Lidén, G. (1997) Physiological response to anaerobicity of
510 glycerol-3-phosphate dehydrogenase mutants of *Saccharomyces cerevisiae*. *Appl Env*
511 *Microbiol* **63**: 128–132.
- 512 Brileya, K. and Reysenbach, A.-L. (2014) The Class *Archaeoglobi*. In *The Prokaryotes*. Springer,
513 Berlin, Heidelberg, pp. 15–23.
- 514 Corliss, J.B. and Ballard, R.D. (1977) Oasis of life in the cold abyss. *Nat Geogr Mag* **152**: 440–453.
- 515 Corre, E., Reysenbach, A.-L., and Prieur, D. (2001) ϵ -Proteobacterial diversity from a deep-sea
516 hydrothermal vent on the Mid-Atlantic Ridge. *FEMS Microbiol Lett* **205**: 329–335.
- 517 Dahle, H., Le Moine Bauer, S., Baumberger, T., Stokke, R., Pedersen, R.B., Thorseth, I.H., and
518 Steen, I.H. (2018) Energy landscapes in hydrothermal chimneys shape distributions of
519 primary producers. *Front Microbiol* **9**.
- 520 Desai, J.V., Bruno, V.M., Ganguly, S., Stamper, R.J., Mitchell, K.F., Solis, N., et al. (2013)
521 Regulatory Role of Glycerol in *Candida albicans* Biofilm Formation. *mBio* **4**.
- 522 Droffner, M.L., Brinton, W.F., and Evans, E. (1995) Evidence for the prominence of well
523 characterized mesophilic bacteria in thermophilic (50–70°C) composting environments.
524 *Biomass Bioenergy* **8**: 191–195.
- 525 Fast, A.G. and Papoutsakis, E.T. (2012) Stoichiometric and energetic analyses of non-photosynthetic
526 CO₂-fixation pathways to support synthetic biology strategies for production of fuels and
527 chemicals. *Curr Opin Chem Eng* **1**: 380–395.
- 528 Fuchs, G. (2011) Alternative Pathways of Carbon Dioxide Fixation: Insights into the Early Evolution
529 of Life? *Annu Rev Microbiol* **65**: 631–658.
- 530 Furdui, C. and Ragsdale, S.W. (2000) The role of pyruvate ferredoxin oxidoreductase in pyruvate
531 synthesis during autotrophic growth by the Wood-Ljungdahl pathway. *J Biol Chem* **275**:
532 28494–28499.
- 533 Hamilton, W.A. (1987) Biofilms: Microbial interactions and metabolic activities. *Ecol Microb*
534 *Communities* 361–385.
- 535 Henstra, A.M., Dijkema, C., and Stams, A.J.M. (2007) *Archaeoglobus fulgidus* couples CO oxidation
536 to sulfate reduction and acetogenesis with transient formate accumulation: The CO
537 metabolism of *A. fulgidus*. *Environ Microbiol* **9**: 1836–1841.
- 538 Hocking, W.P., Roalkvam, I., Magnussen, C., Stokke, R., and Steen, I.H. (2015) Assessment of the
539 Carbon Monoxide Metabolism of the Hyperthermophilic Sulfate-Reducing Archaeon
540 *Archaeoglobus fulgidus* VC-16 by Comparative Transcriptome Analyses. *Archaea* **2015**: 1–
541 12.
- 542 Huber, H. and Stetter, K.O. (2015) Desulfurococcales ord. nov. In *Bergey's Manual of Systematics*
543 *of Archaea and Bacteria*. American Cancer Society, pp. 1–2.
- 544 Huber, J.A., Butterfield, D.A., and Baross, J.A. (2003) Bacterial diversity in a seafloor habitat
545 following a deep-sea volcanic eruption. *FEMS Microbiol Ecol* **43**: 393–409.
- 546 Huber, J.A., Butterfield, D.A., and Baross, J.A. (2002) Temporal changes in archaeal diversity and
547 chemistry in a mid-ocean ridge seafloor habitat. *Appl Environ Microbiol* **68**: 1585–1594.

- 548 Ishii, T., Kawaichi, S., Nakagawa, H., Hashimoto, K., and Nakamura, R. (2015) From
549 chemolithoautotrophs to electrolithoautotrophs: CO₂ fixation by Fe(II)-oxidizing bacteria
550 coupled with direct uptake of electrons from solid electron sources. *Front Microbiol* **6**.
551 Jaeschke, A., Jørgensen, S.L., Bernasconi, S.M., Pedersen, R.B., Thorseth, I.H., and Früh-Green,
552 G.L. (2012) Microbial diversity of Loki's Castle black smokers at the Arctic Mid-Ocean
553 Ridge. *Geobiology* **10**: 548–561.
554 Jia, R., Yang, D., Xu, D., and Gu, T. (2018) Carbon steel biocorrosion at 80 °C by a thermophilic
555 sulfate reducing archaeon biofilm provides evidence for its utilization of elemental iron as
556 electron donor through extracellular electron transfer. *Corros Sci* **145**: 47–54.
557 Kato, S., Hashimoto, K., and Watanabe, K. (2012) Microbial interspecies electron transfer via
558 electric currents through conductive minerals. *Proc Natl Acad Sci* **109**: 10042–10046.
559 Lai, B., Yu, S., Bernhardt, P.V., Rabaey, K., Virdis, B., and Krömer, J.O. (2016) Anoxic metabolism
560 and biochemical production in *Pseudomonas putida* F1 driven by a bioelectrochemical
561 system. *Biotechnol Biofuels* **9**: 39.
562 Lim, S.S., Yu, E.H., Daud, W.R.W., Kim, B.H., and Scott, K. (2017) Bioanode as a limiting factor
563 to biocathode performance in microbial electrolysis cells. *Bioresour Technol* **238**: 313–324.
564 Lin, T.J., Ver Eecke, H.C., Breves, E.A., Dyar, M.D., Jamieson, J.W., Hannington, M.D., et al.
565 (2016) Linkages between mineralogy, fluid chemistry, and microbial communities within
566 hydrothermal chimneys from the Endeavour Segment, Juan de Fuca Ridge:
567 GEOMICROBIOLOGY OF HYDROTHERMAL CHIMNEYS. *Geochem Geophys*
568 *Geosystems* **17**: 300–323.
569 Lovley, D.R. (2017) Syntrophy goes electric: Direct interspecies electron transfer. *Annu Rev*
570 *Microbiol* **71**: 643–664.
571 Lyons, C.M., Justin, P., Colby, J., and Williams, E. (1984) Isolation, characterization and autotrophic
572 metabolism of a moderately thermophilic carboxydobacterium, *Pseudomonas*
573 *thermocarboxydovorans* sp. nov. *Microbiology* **130**: 1097–1105.
574 Manzella, M.P., Holmes, D.E., Rocheleau, J.M., Chung, A., Reguera, G., and Kashefi, K. (2015) The
575 complete genome sequence and emendation of the hyperthermophilic, obligate iron-reducing
576 archaeon “Geoglobus ahangari” strain 234T. *Stand Genomic Sci* **10**: 77.
577 Marshall, C.W., Ross, D.E., Fichot, E.B., Norman, R.S., and May, H.D. (2013) Long-term Operation
578 of Microbial Electrosynthesis Systems Improves Acetate Production by Autotrophic
579 Microbiomes. *Environ Sci Technol* **47**: 6023–6029.
580 Maruthupandy, M., Anand, M., Maduraiveeran, G., Beevi, A.S.H., and Priya, R.J. (2015) Electrical
581 conductivity measurements of bacterial nanowires from *Pseudomonas aeruginosa*. *Adv Nat*
582 *Sci Nanosci Nanotechnol* **6**: 045007.
583 Nercessian, O., Reysenbach, A.-L., Prieur, D., and Jeanthon, C. (2003) Archaeal diversity associated
584 with in situ samplers deployed on hydrothermal vents on the East Pacific Rise (13°N).
585 *Environ Microbiol* **5**: 492–502.
586 Palleroni, N.J. (2015) *Pseudomonas*. In *Bergey's Manual of Systematics of Archaea and Bacteria*.
587 American Cancer Society, pp. 1–1.
588 Pillot, G., Davidson, S., Auria, R., Combet-Blanc, Y., Godfroy, A., and Liebgott, P.-P. (2019)
589 Production of Current by Syntrophy Between Exoelectrogenic and Fermentative
590 Hyperthermophilic Microorganisms in Heterotrophic Biofilm from a Deep-Sea
591 Hydrothermal Chimney. *Microb Ecol*.
592 Pillot, G., Frouin, E., Pasero, E., Godfroy, A., Combet-Blanc, Y., Davidson, S., and Liebgott, P.-P.
593 (2018) Specific enrichment of hyperthermophilic electroactive *Archaea* from deep-sea
594 hydrothermal vent on electrically conductive support. *Bioresour Technol* **259**: 304–311.
595 Pous, N., Carmona-Martínez, A.A., Vilajeliu-Pons, A., Fiset, E., Bañeras, L., Trably, E., et al. (2016)
596 Bidirectional microbial electron transfer: Switching an acetate oxidizing biofilm to nitrate
597 reducing conditions. *Biosens Bioelectron* **75**: 352–358.
598 Reimers, C.E., Girguis, P., Stecher, H.A., Tender, L.M., Ryckelynck, N., and Whaling, P. (2006)
599 Microbial fuel cell energy from an ocean cold seep. *Geobiology* **4**: 123–136.

- 600 Reysenbach, A.-L., Longnecker, K., and Kirshtein, J. (2000) Novel bacterial and archaeal lineages
601 from an in situ growth chamber deployed at a Mid-Atlantic Ridge hydrothermal vent. *Appl*
602 *Environ Microbiol* **66**: 3798–3806.
- 603 Salter, S.J., Cox, M.J., Turek, E.M., Calus, S.T., Cookson, W.O., Moffatt, M.F., et al. (2014) Reagent
604 and laboratory contamination can critically impact sequence-based microbiome analyses.
605 *BMC Biol* **12**: 87.
- 606 Sarradin, P.-M. and Cannat, M. (2014) MOMARSAT2014 cruise, Pourquoi pas ? R/V.
- 607 Schleucher, J., Schwendinger, M., Sattler, M., Schmidt, P., Schedletzky, O., Glaser, S.J., et al. (1994)
608 A general enhancement scheme in heteronuclear multidimensional NMR employing pulsed
609 field gradients. *J Biomol NMR* **4**: 301–306.
- 610 Schrenk, M.O., Kelley, D.S., Delaney, J.R., and Baross, J.A. (2003) Incidence and diversity of
611 microorganisms within the walls of an active deep-sea sulfide chimney. *Appl Environ*
612 *Microbiol* **69**: 3580–3592.
- 613 Shemesh, M. and Chai, Y. (2013) A Combination of Glycerol and Manganese Promotes Biofilm
614 Formation in *Bacillus subtilis* via Histidine Kinase KinD Signaling. *J Bacteriol* **195**: 2747–
615 2754.
- 616 Shen, H.-B., Yong, X.-Y., Chen, Y.-L., Liao, Z.-H., Si, R.-W., Zhou, J., et al. (2014) Enhanced
617 bioelectricity generation by improving pyocyanin production and membrane permeability
618 through sophorolipid addition in *Pseudomonas aeruginosa*-inoculated microbial fuel cells.
619 *Bioresour Technol* **167**: 490–494.
- 620 Sokolova, T. and Lebedinsky, A. (2013) CO-Oxidizing Anaerobic Thermophilic Prokaryotes. In
621 *Thermophilic Microbes in Environmental and Industrial Biotechnology: Biotechnology of*
622 *Thermophiles*. Satyanarayana, T., Littlechild, J., and Kawarabayasi, Y. (eds). Dordrecht:
623 Springer Netherlands, pp. 203–231.
- 624 Takai, K., Gamo, T., Tsunogai, U., Nakayama, N., Hirayama, H., Nealson, K.H., and Horikoshi, K.
625 (2004) Geochemical and microbiological evidence for a hydrogen-based, hyperthermophilic
626 subsurface lithoautotrophic microbial ecosystem (HyperSLiME) beneath an active deep-sea
627 hydrothermal field. *Extremophiles* **8**: 269–282.
- 628 Vorholt, J.A., Hafenbradl, D., Stetter, K.O., and Thauer, R.K. (1997) Pathways of autotrophic CO₂
629 fixation and of dissimilatory nitrate reduction to N₂ O in *Ferroglobus placidus*. *Arch*
630 *Microbiol* **167**: 19–23.
- 631 Vos, P.D. (2015) Bacillales. In *Bergey's Manual of Systematics of Archaea and Bacteria*. American
632 Cancer Society, pp. 1–1.
- 633 Wirth, R. (2017) Colonization of black smokers by hyperthermophilic microorganisms. *Trends*
634 *Microbiol* **25**: 92–99.
- 635 Wirth, R., Luckner, M., and Wanner, G. (2018) Validation of a hypothesis: Colonization of black
636 smokers by hyperthermophilic microorganisms. *Front Microbiol* **9**: 524.
- 637 Yamamoto, M., Nakamura, R., Kasaya, T., Kumagai, H., Suzuki, K., and Takai, K. (2017)
638 Spontaneous and Widespread Electricity Generation in Natural Deep-Sea Hydrothermal
639 Fields. *Angew Chem Int Ed* **56**: 5725–5728.
- 640 Yilmazel, Y.D., Zhu, X., Kim, K.-Y., Holmes, D.E., and Logan, B.E. (2018) Electrical current
641 generation in microbial electrolysis cells by hyperthermophilic archaea *Ferroglobus*
642 *placidus* and *Geoglobus ahangari*. *Bioelectrochemistry* **119**: 142–149.
- 643 Zhang, L., Kang, M., Xu, Jiajun, Xu, Jian, Shuai, Y., Zhou, X., et al. (2016) Bacterial and archaeal
644 communities in the deep-sea sediments of inactive hydrothermal vents in the Southwest India
645 Ridge. *Sci Rep* **6**:
646

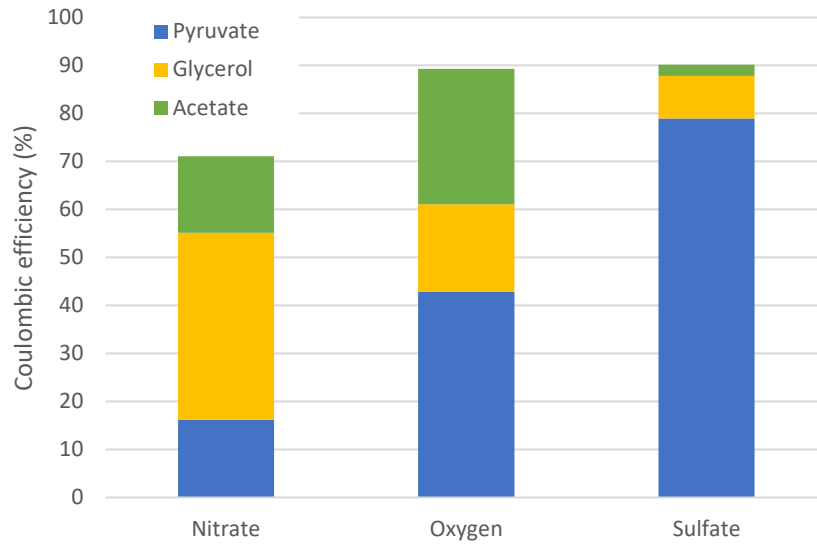
647

648 **Figures**



652 **Figure 1.** Current consumption (red continuous line); pyruvate (blue triangle), glycerol (yellow
653 square) and acetate (green cross) productions over time of culture for each electron-acceptor
654 experiment. The current was obtained from a poised electrode at -590 mV vs SHE for nitrate and
655 sulfate experiments and -300 mV vs SHE for oxygen.

656

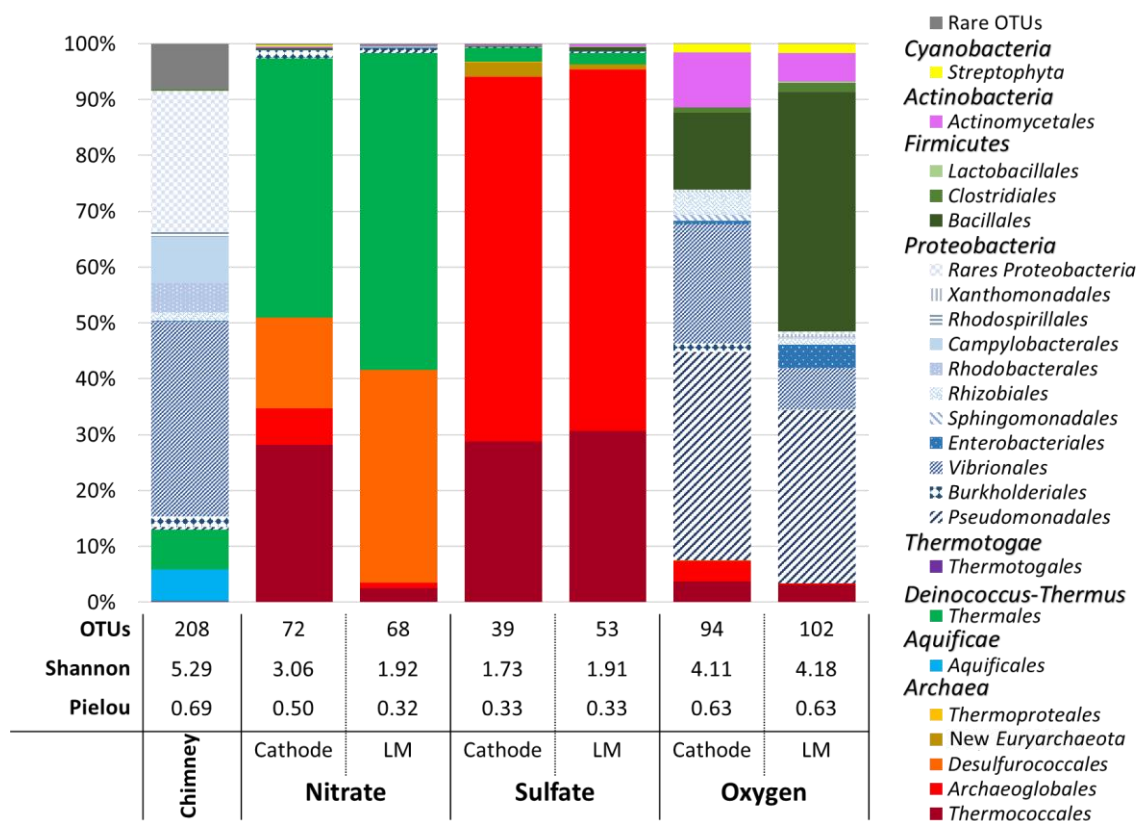


657

658 **Figure 2.** Coulombic efficiency for organic products in presence of the different electron

659 acceptors.

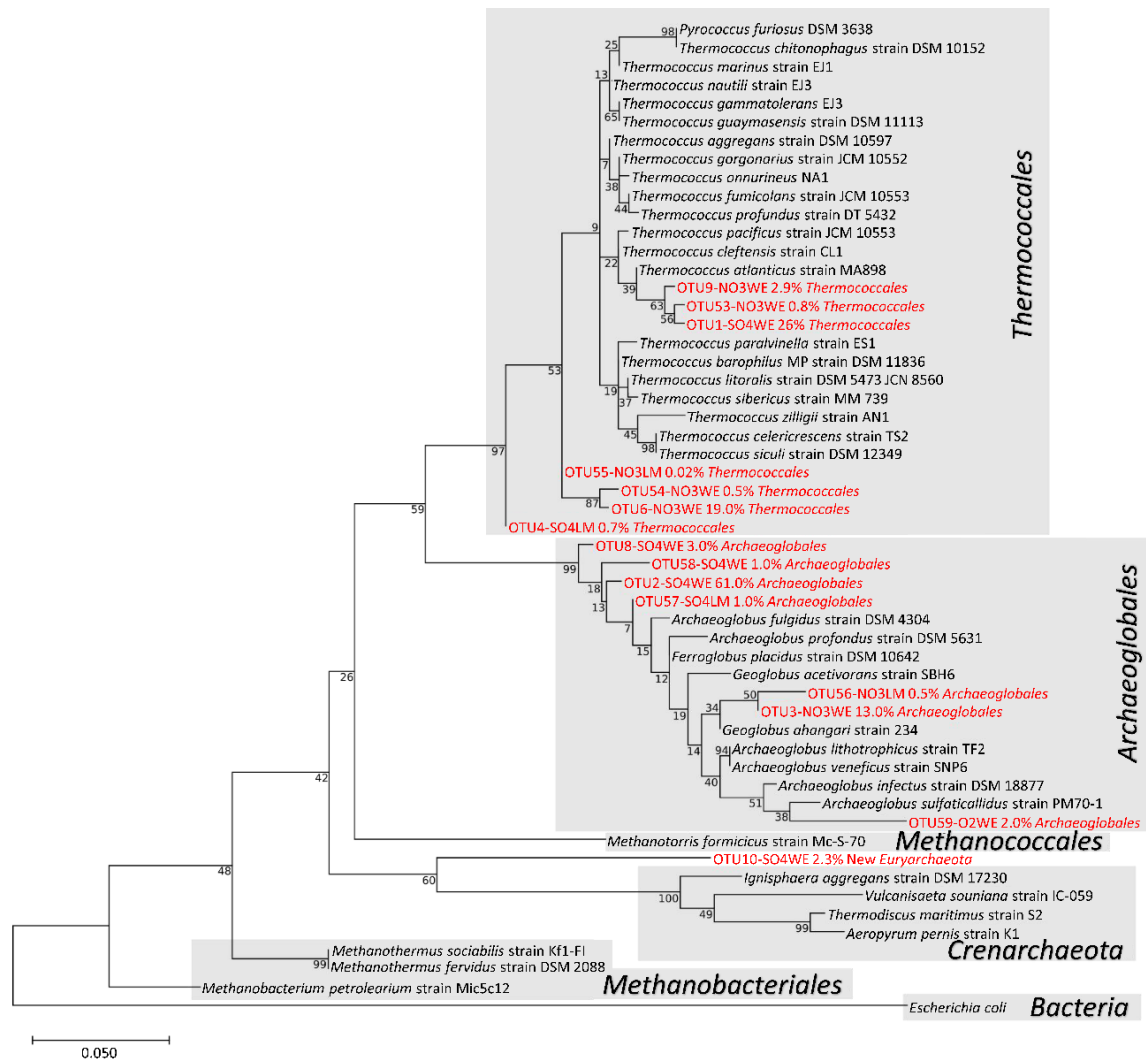
660



661
 662 **Figure 3.** Dominant taxonomic affiliation at order level and biodiversity indices of microbial
 663 communities from a crushed chimney sample from Capelinhos vent site (Lucky Strike
 664 hydrothermal vent field), as plotted on the cathode and liquid media (LM) after the weeks of
 665 culture. OTUs representing less than 1% of total sequences of the samples are pooled as 'Rare
 666 OTUs'.

667

668

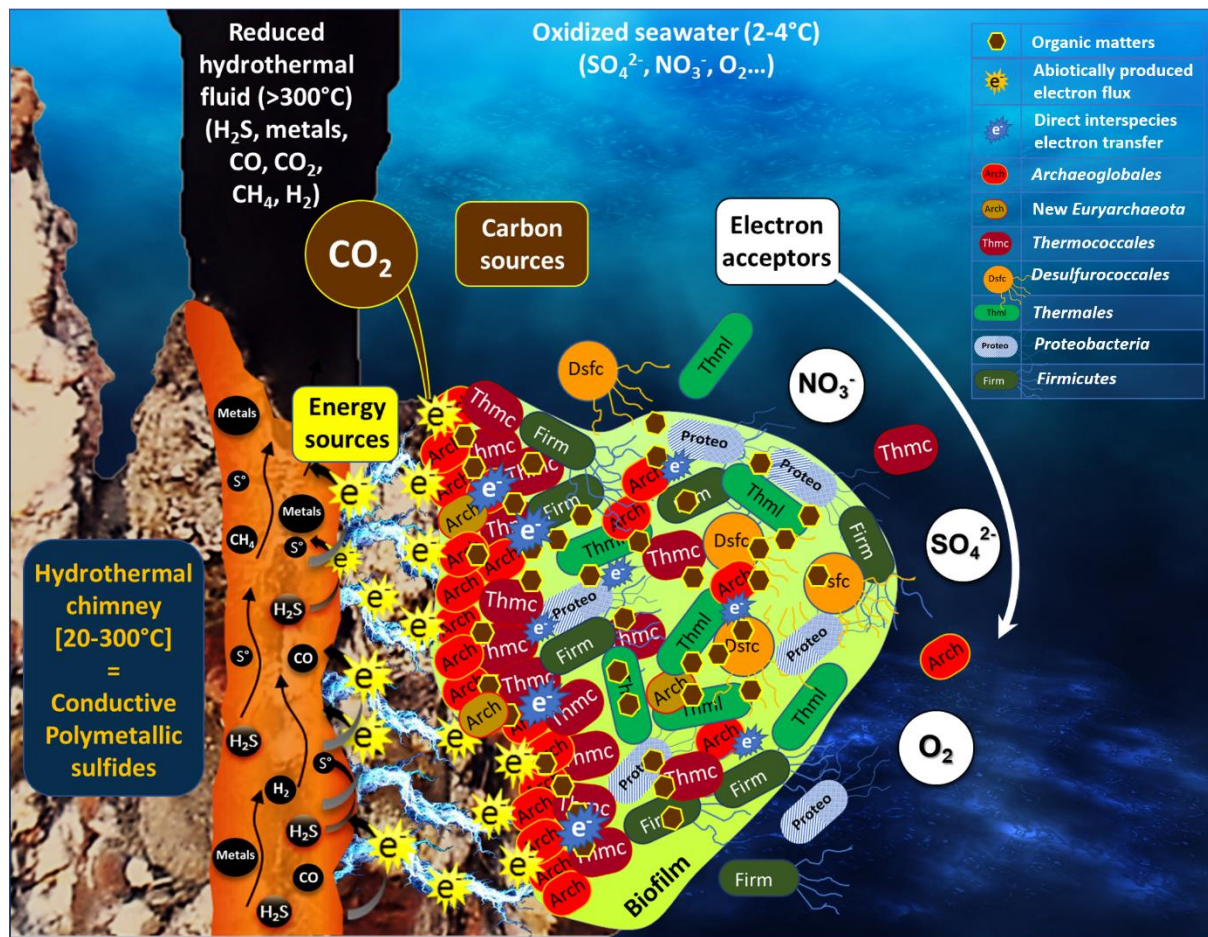


669 **Figure 4.** Maximum Likelihood phylogenetic tree of archaeal OTUs retrieved on various
670 enrichments on the 293pb 16S fragment obtained in the barcoding 16S method (LM: Liquid
671 Media; WE: Working Electrode, cathode). Numbers at nodes represent bootstrap values inferred
672 by MEGAX. Scale bars represent the average number of substitutions per site.

673

674

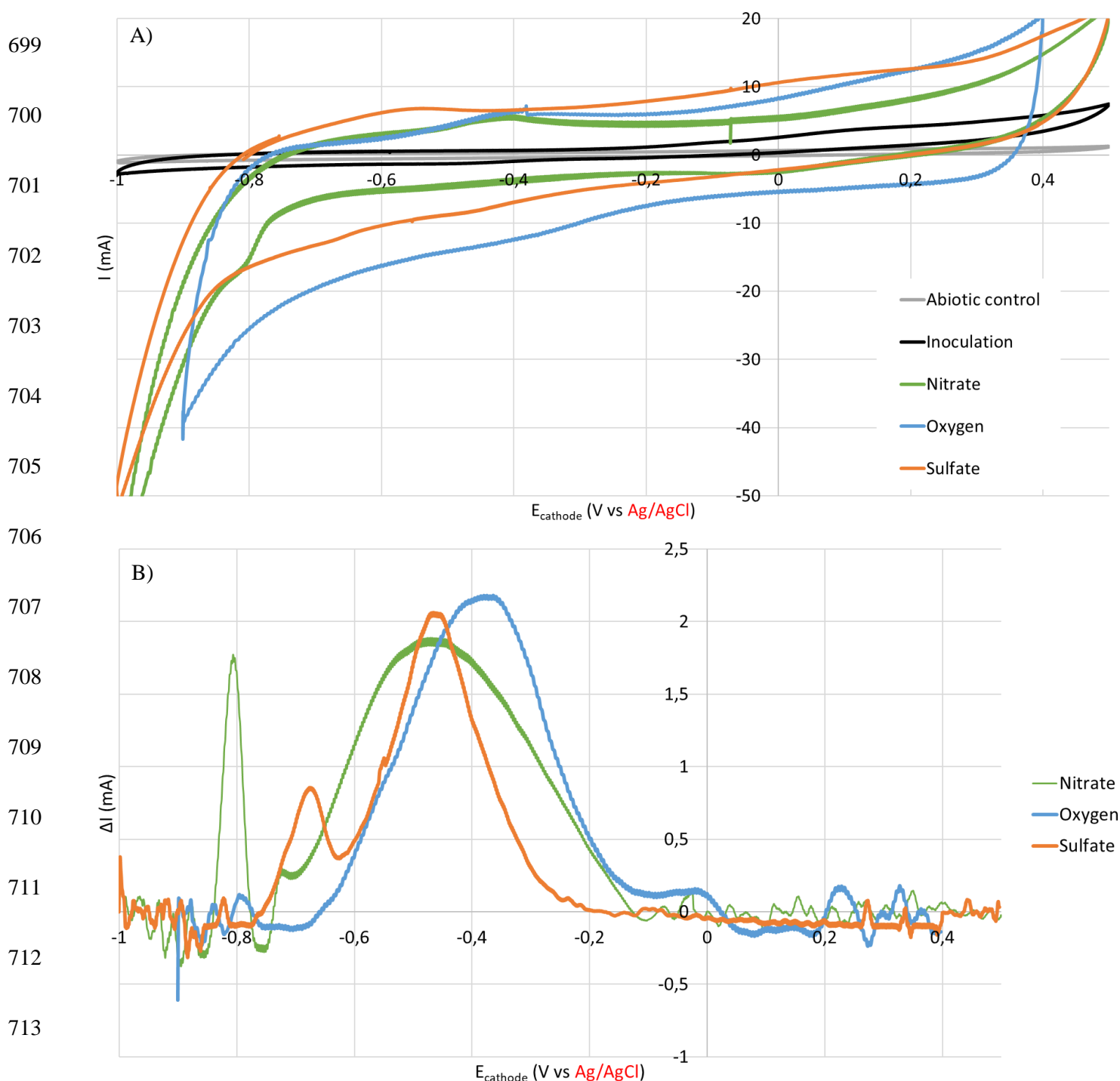
675



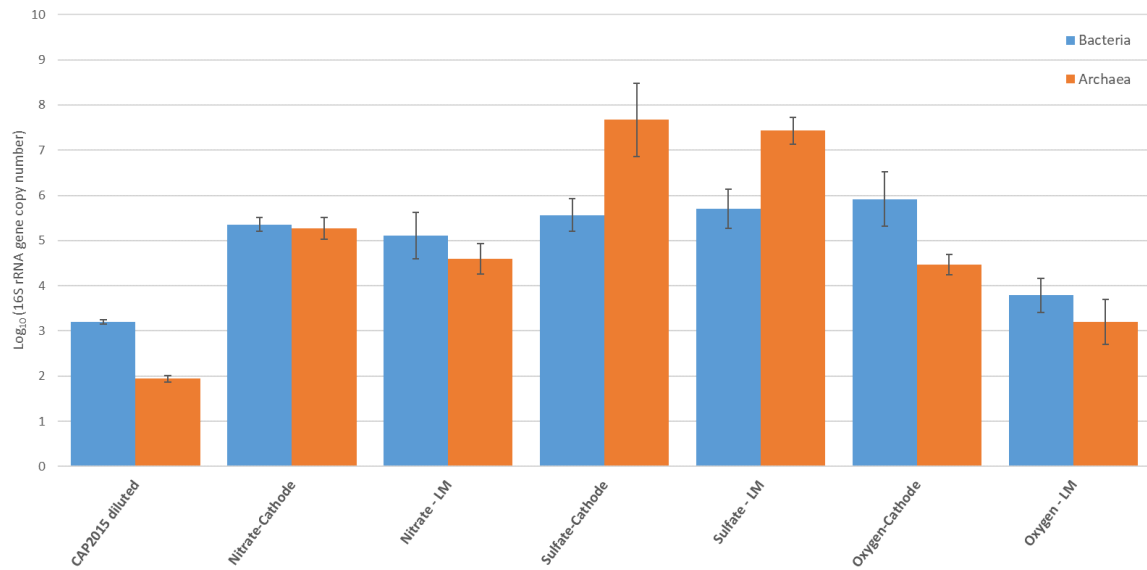
676

677 Figure 5: Schematic representation of microbial colonization of iron-rich hydrothermal
 678 chimney (Capelinhos site on the Lucky Strike hydrothermal field) by
 679 electrolithoautotrophic microorganisms. The production of an abiotic electrical current by
 680 potential differences between the reduced hydrothermal fluid (H_2S , metals, CO , CH_4 , H_2 ...)
 681 and oxidized seawater (O_2 , SO_4^{2-} , NO_3^{-}) (Yamamoto et al. 2017) leads to the formation of
 682 electron flux moving towards the chimney surface. This electrons flux can serve directly as
 683 an energy source to enable the growth of electrolithoautotrophic and hyperthermophilic
 684 *Archaeoglobales* using the CO_2 as carbon source and nitrate and/or sulfate as electron
 685 acceptors. In the absence of a usable electron acceptor, *Archaeoglobales* would be likely
 686 to perform direct interspecies electron transfer to ensure their growth. The electron
 687 acceptor fluctuations, correlated to the continual influx of electric current would favor the
 688 production of organic matters (amino acid, formate, pyruvate, glycerol...) by the
 689 *Archaeoglobales*. This organic matter is then used by heterotrophic microorganisms by
 690 fermentation or respiration (anaerobic or aerobic) thus providing the primal food web
 691 initially present into the hydrothermal ecosystems. *The electrical current also could favor*
 692 *the electrolysis water leading to the abiotic H_2 production (not measurable in our abiotic*
 693 *conditions), which would serve as chemical energy source.* Arch: *Archaeoglobales*; Thmc:
 694 *Thermococcales*; Dsfc: *Desulfurococcales*; Thml: *Thermales*; Prot: *Proteobacteria*; Firm:
 695 *Firmicute*; NO_3^{-} : nitrate; SO_4^{2-} : sulfate; O_2 : dioxygen; CH_4 : Methane; CO_2 : Carbon Dioxide;
 696 CO : Carbon monoxide; H_2S : Hydrogen sulfide ; S° : sulfur; Metals: Fe, Mn, Cu, Zn...
 697

698 SUPPLEMENTARY INFORMATION



714 **Supplementary Information Figure S1:** A) Cyclic Voltammograms (scan rate = 20 mV/s) of the abiotic
715 control, and of the experiments at inoculation time and after 30 days for each condition (Nitrate, Oxygen and
716 Sulfate). B) Reduction peaks extracted from Cyclic Voltammograms (scan rate = 20 mV/s) where the baseline
717 have been subtracted with the software QSoas. The ΔI of reduction peaks are expressed in inversed values.
Cyclic voltammograms carried out with a 3 M Ag/AgCl reference electrode ($E = +0.165$ V vs SHE at 80°C).

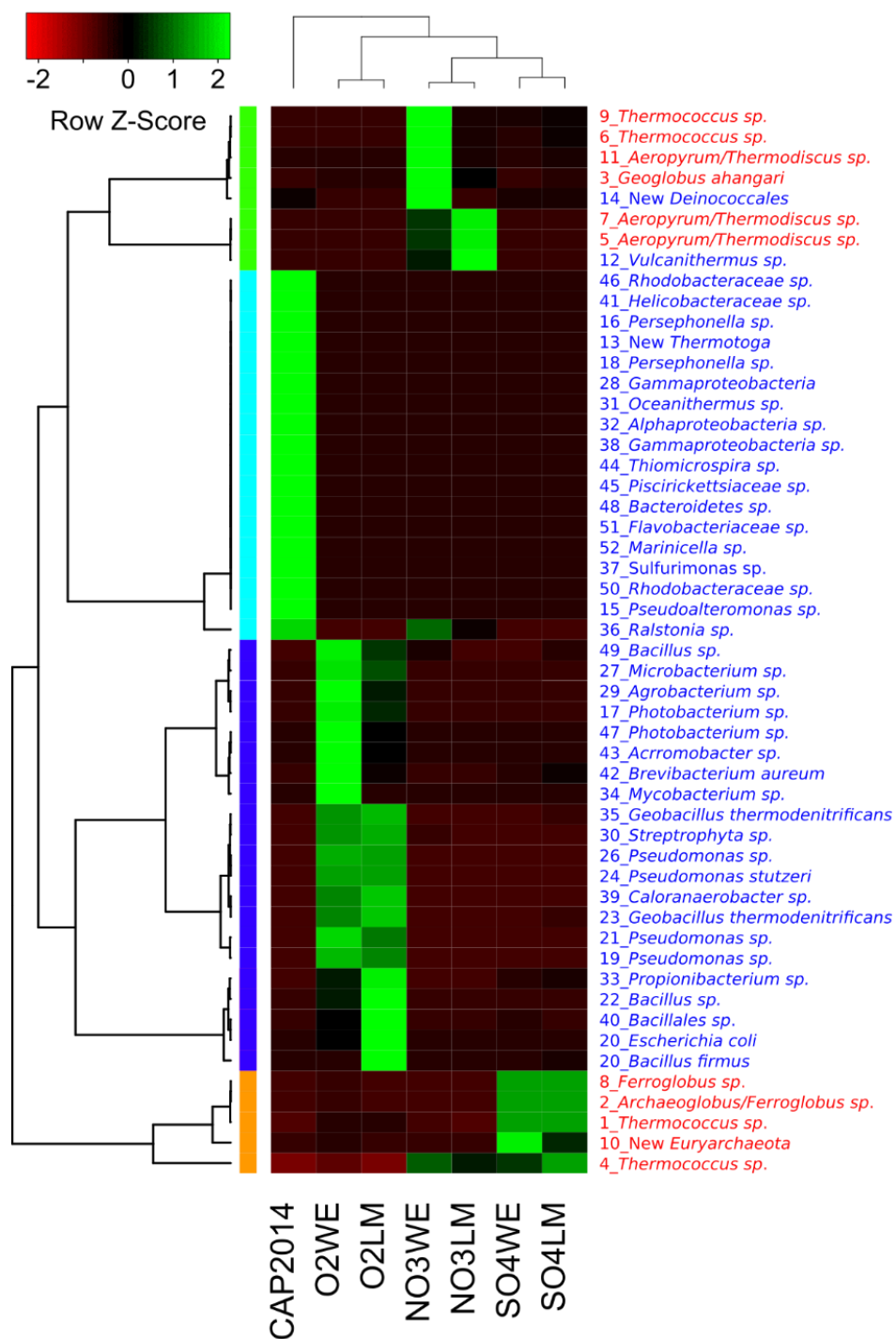


718

719 **Supplementary Information Figure S2.** Quantification of 16S rRNA gene copies from Bacteria

720 (blue) or Archaea (orange) per gram of crushed chimney, per milliliter of liquid or per cm² of

721 working electrode. Error bar represent the standard deviation obtained on triplicates.



722

723 **Supplementary Information Figure S3.** Heatmap representation of the distribution of dominant

724 OTUs (>0.05%) over the different electron acceptors (LM: Liquid Media; WE: Working Electrode,

725 cathode). OTUs and samples clustering were performed with centroid average method and with

726 Pearson distance measurement method. The red taxa represent the Archaea members and blue

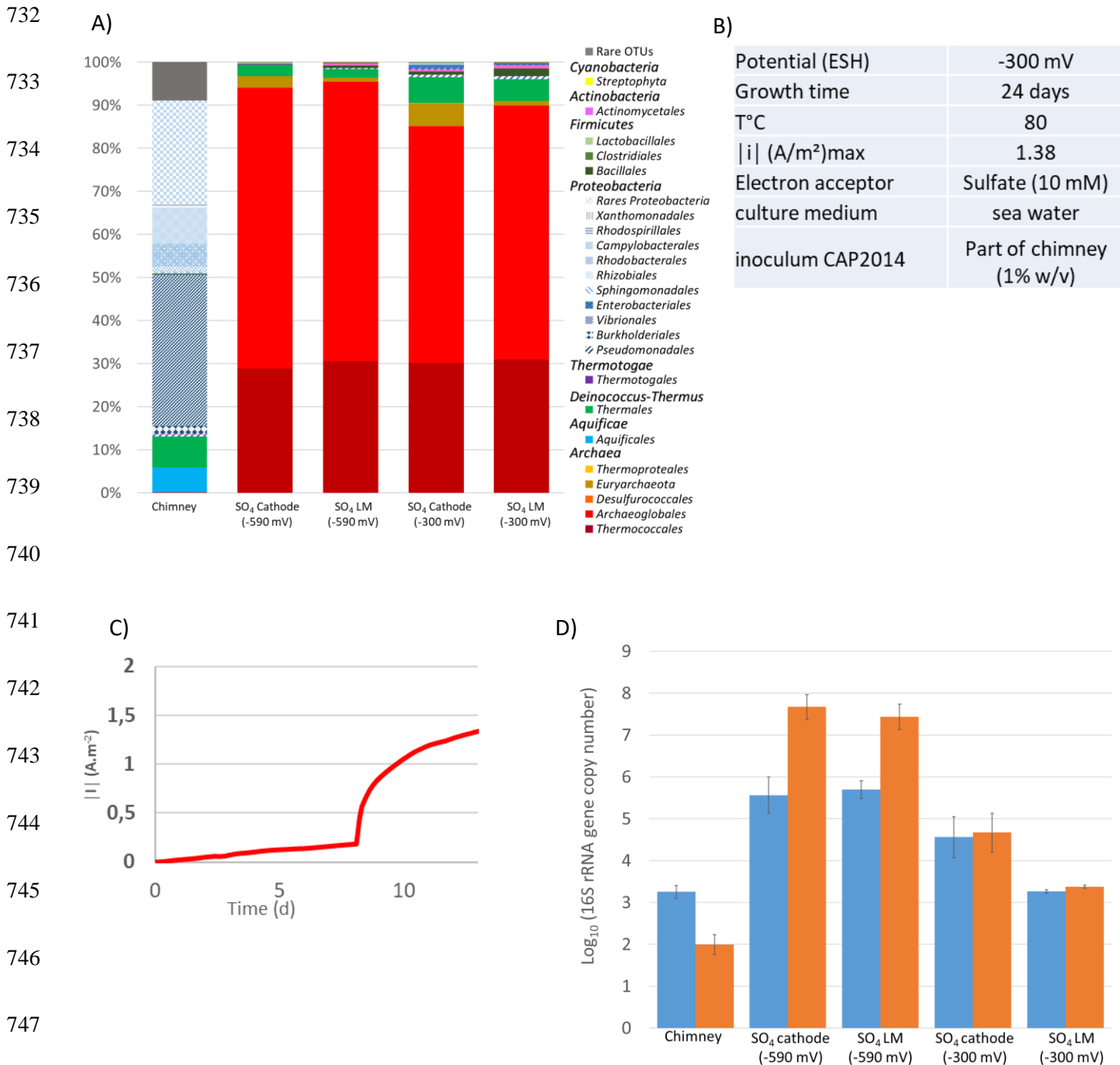
727 taxa, the Bacteria.

728

729

730

731



Supplementary Information Figure S4: A) Biodiversity comparisons developing it on poised cathode at -590 mV and -300 mV vs SHE in presence of sulfate. B) Parameters of growth with the cathode poised at -300 mV vs SHE. C) current consumption correlated to the growth of biofilm. D) Quantification of 16S rRNA gene copies from Bacteria (blue) or Archaea (orange) per gram of crushed chimney, per milliliter of liquid or per cm² of cathode.

753

754

755

756

757

758

759

760

761

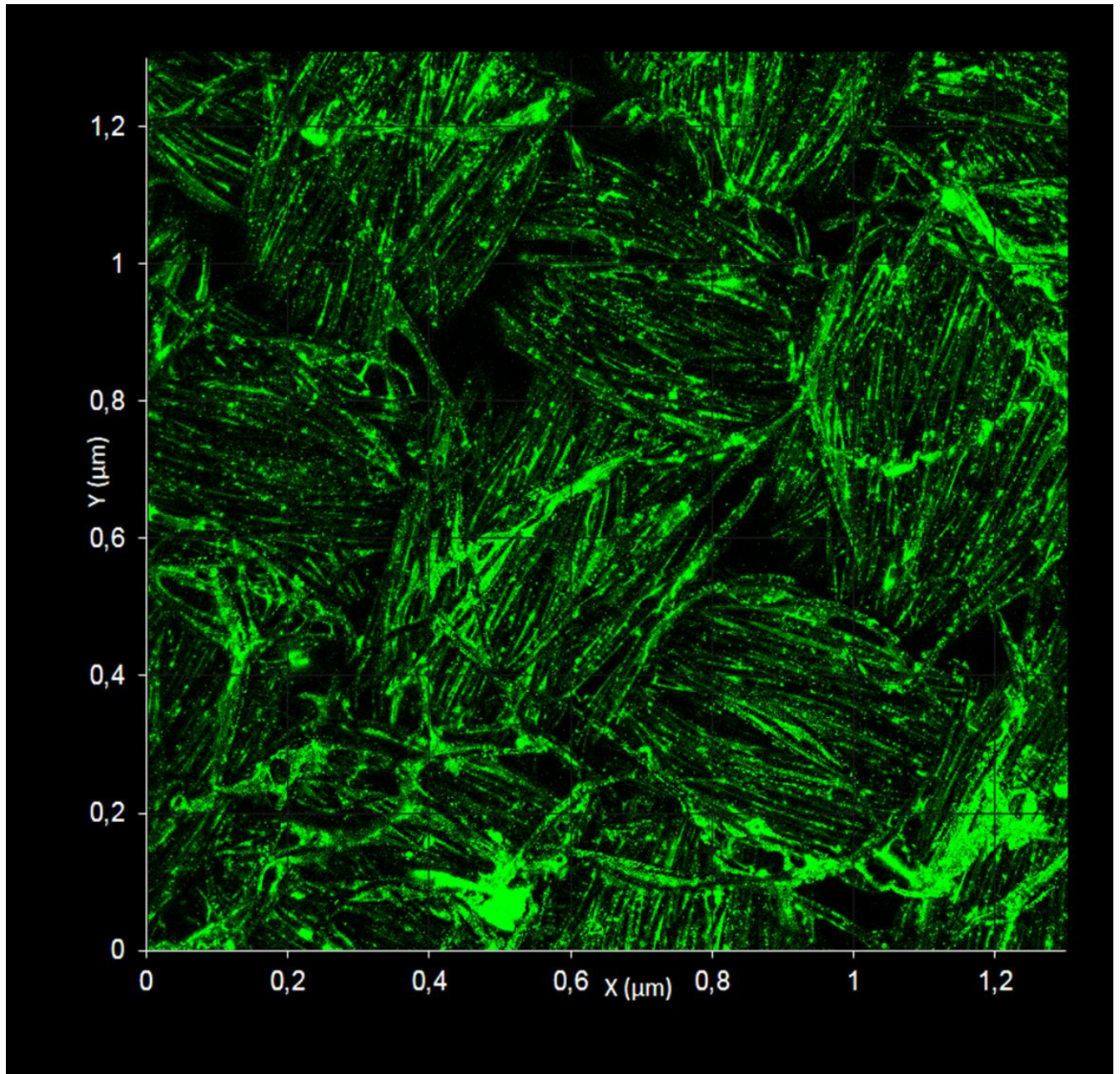
762

763

764

765

766



767

768

Supplementary information Figure S5: Representative confocal microscopy of the biofilm after 30 days of experiment on nitrate as electron acceptor. The green signal, corresponding to cells stained with Syto9 dye, allow to show the biofilm covering the interwoven carbon fibers.

770

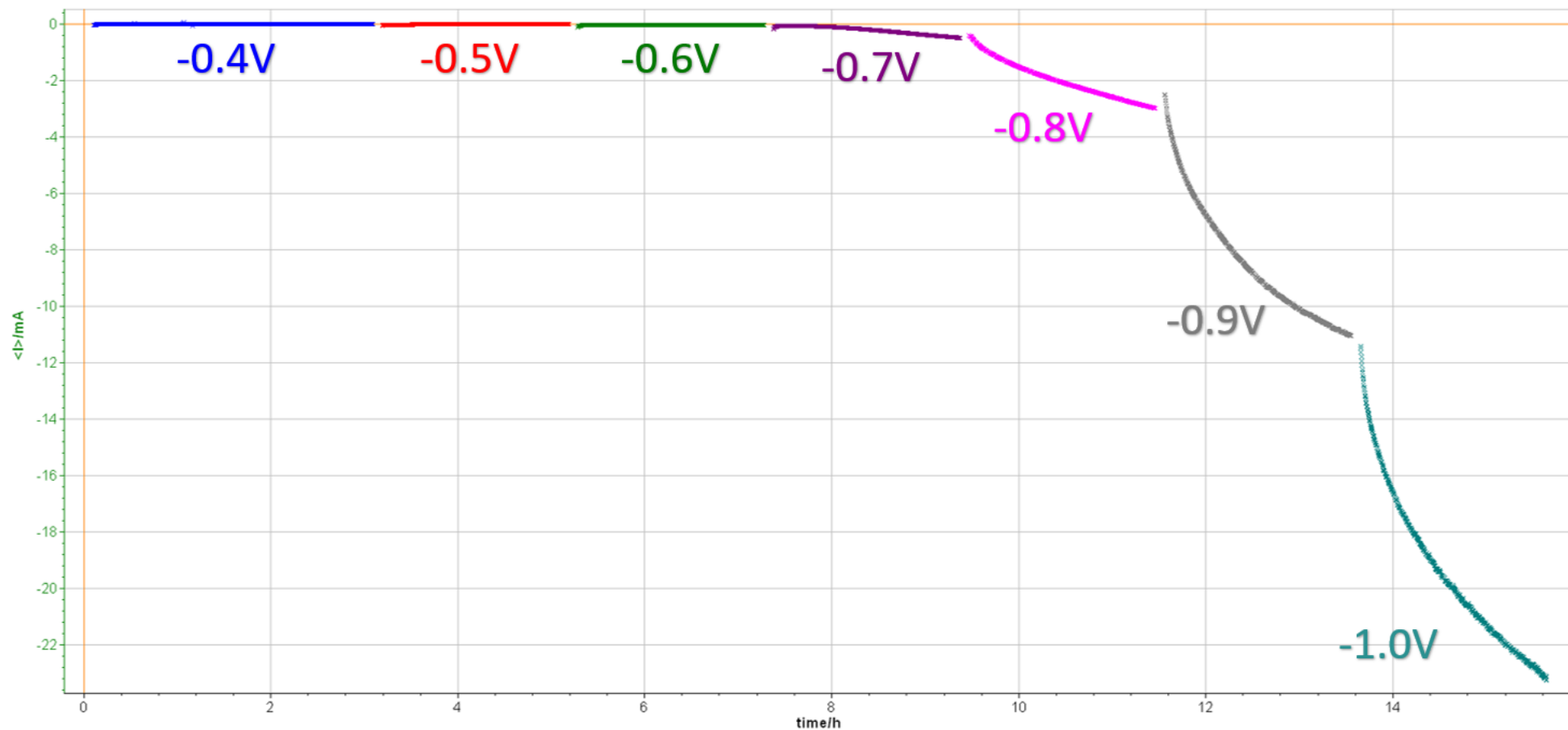
771

772

Time (days)	Benzoate like	Methanol	Formate	Cystine	Acetoacetate	Lactate	Threonine	Succinate	Ethanol	Alanine	Acetamide	2-Aminoisobutyric acid	3-hydroxyisovalerate
0	0,0056	0,0032	0,0085	0,0123	0,024	0,0066	0,0019	0,0013	0,0022	0	0	0,0048	0,0046
1	0	0	0,0615	0,0355	0	0,03	0,0115	0	0,177	0	0	0,067	0,0375
2	0,0294	0	0,0084	0,0302	0	0,024	0,0026	0,0022	0,0406	0	0	0	0,0076
3	0,0198	0,0108	0,0549	0,0237	0	0,015	0,0036	0	0,0375	0,0108	0	0,0051	0,0282
4	0,0242	0,1606	0,0218	0,0306	0	0,0106	0,004	0	0,0425	0,012	0,02	0,0042	0,0066
5	0,0255	0,0315	0,0705	0,0236	0	0,0315	0,003	0	0,0475	0,0105	0,0255	0,0065	0,0345
7	0,0544	0,009	0,0234	0,0177	0	0,0092	0,0042	0	0,0298	0,0138	0,0486	0,0152	0,0094
9	0,055	0,036	0,063	0,0138	0,044	0,037	0	0	0,086	0	0,054	0,028	0,081
11	0,0766	0,0092	0,0258	0,0096	0,0046	0,011	0,0022	0	0,0168	0,0202	0,0576	0,0196	0,0138
12	0,0762	0	0,017	0,0078	0,0154	0,0122	0,002	0	0	0	0,0692	0,0216	0,008
13	0,0948	0	0,0326	0,0012	0	0,0172	0	0	0,0336	0,0542	0,0394	0,012	0,0144
15	0,1034	0,0072	0,0236	0,0026	0	0,016	0,002	0	0	0,0936	0,0358	0,0132	0,0112
16	0,1161	0	0	0	0	0,0276	0,0087	0	0,0579	0,1785	0,0189	0,0081	0,0234
18	0,099	0,0046	0,0134	0	0	0,011	0,0012	0	0	0,1798	0,0106	0	0,0098
21	0,1284	0,0054	0,022	0,0194	0	0,013	0,004	0,0012	0,0064	0,2366	0,0064	0	0,0146

773 **Supplementary information Table 1:** Evolution of transient compounds (in mM) over the enrichment on Nitrate measured by NMR

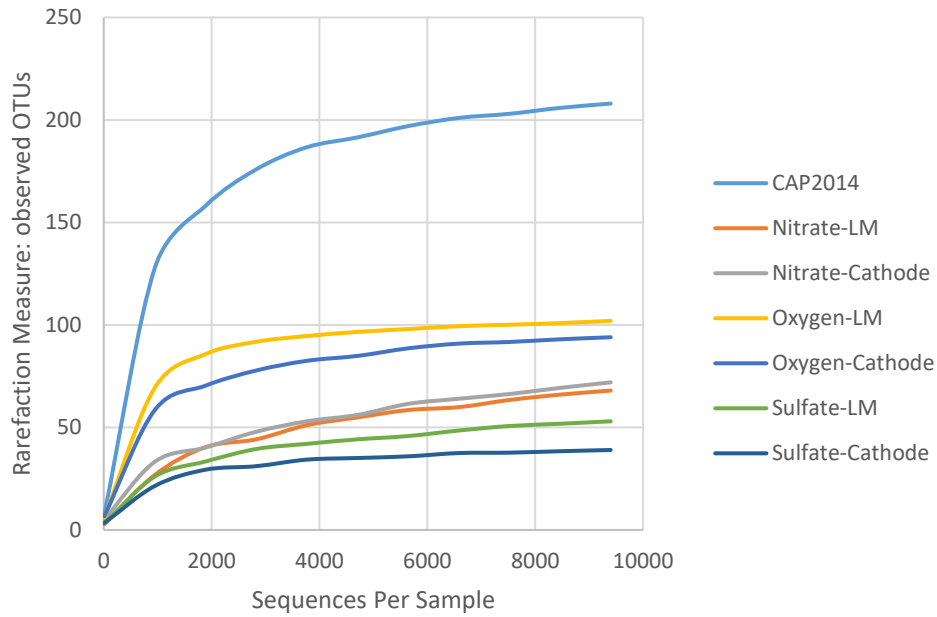
774



775

776 **Supplementary information Figure S6:** Screening of potentials in abiotic and anaerobic conditions to select the lowest potential before water electrolysis.

777 Potential are expressed vs. SHE.



778

779 **Supplementary Information Figure S7.** Rarefaction curves of 16S rDNA sequences for bacterial

780 and archaeal diversities in the different samples. Curves were calculated on OTUs at 97%

781 similarity.

782

783